Defective cell-autonomous signalling and antigenic polyreactivity of B-cell receptors from chronic lymphocytic leukaemia stereotyped subset 1

P. G. Cocomazzi, A. Iatrou, C. Minici et al.

Supplementary material

Contents:

A

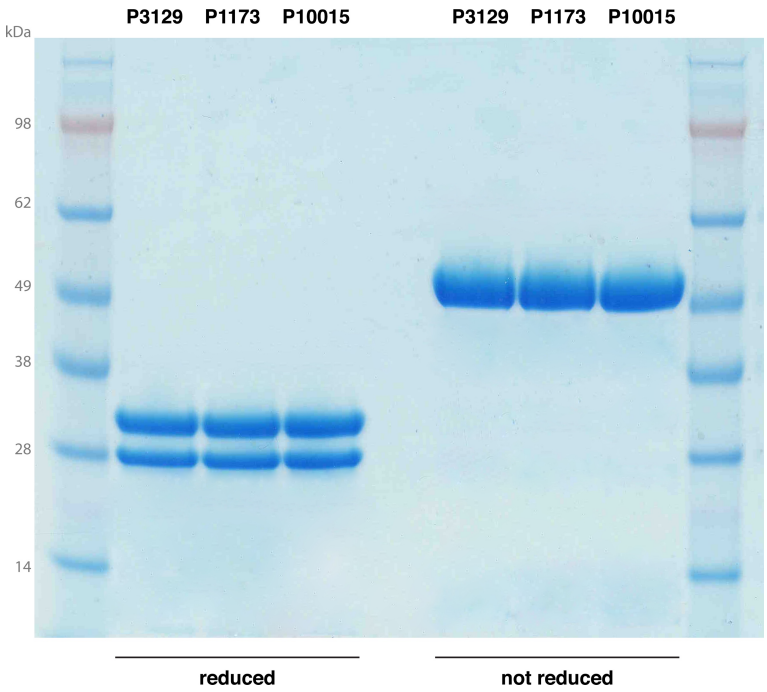

B

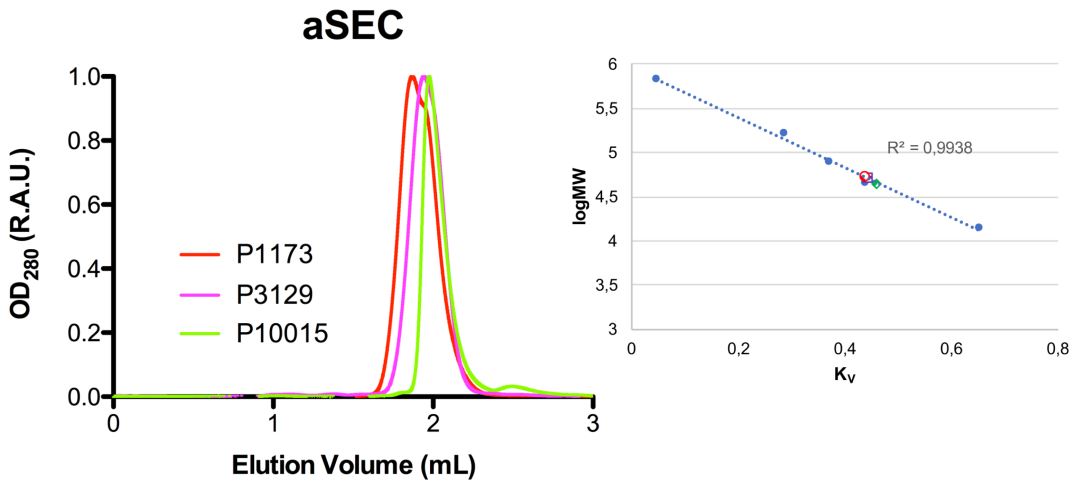

Figure S1. Purity and oligomeric state of the crystallized CLL subset 1 BCR Fabs. **A,** Coomassie-stained SDS-PAGE analysis of the purified Fabs for which the crystal structure was determined. **B,** Size exclusion chromatographic analysis of the P3129, P10015 and P1173 BCR Fabs, showing the elution of a single species with a calculated MW of 49 kDa based on the calibration curve.

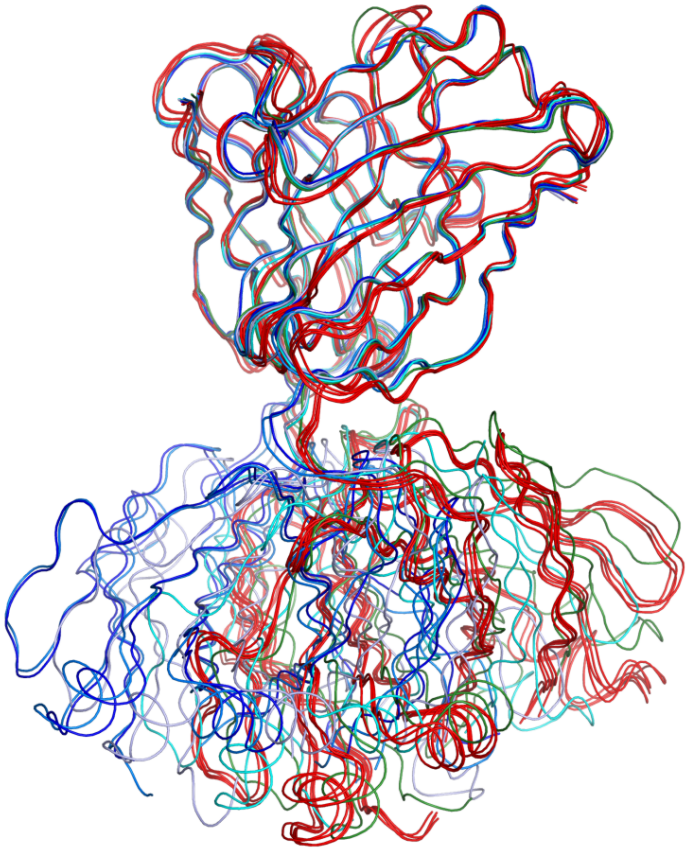

Figure S2. Elbow angle variability in the crystallized subset 1 BCR Fabs. The crystallographic-independent molecules of subset 1 BCR Fabs P3129 (four molecules, coloured in shades of blue), P10015 (one molecule, green) and P1173 (four molecules, red) were superimposed using the variable domains of the heavy and light chains, and are shown as a thin tube. The constant domains, in the bottom part of the figure, span a wide range of orientations.

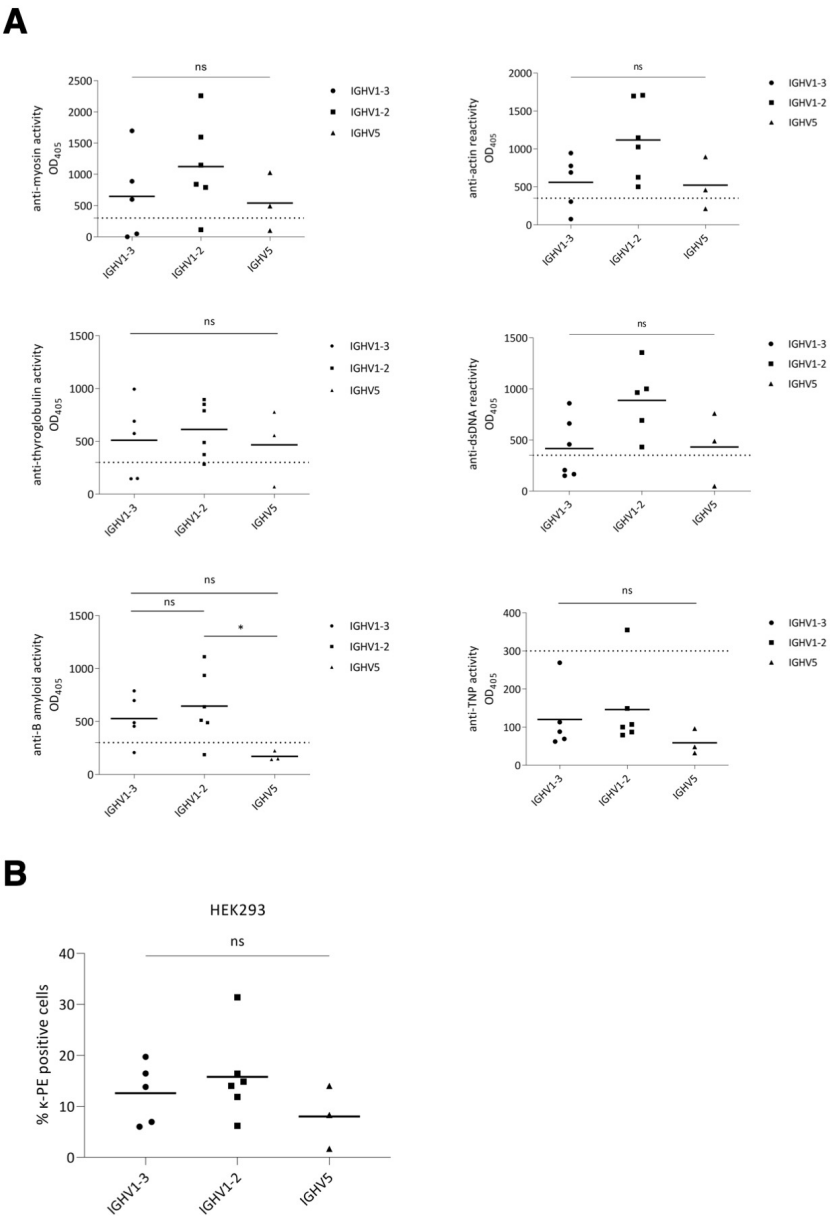

Figure S3. Similar antigenic reactivity of subset 1 rmAbs using different IGHV genes. **A**, the reactivity towards the indicated antigens, also shown in the main text, is clustered based on IGHV1-3, IGHV1-2 or IGHV1-5 usage in the BCRs. Dashed horizontal lines indicate the detection limit for positive reactivity. **B**, observed subset 1 rmAb reactivity towards human embryonic kidney cells clustered according to heavy chain gene usage. ns, statistically non-significant differences.

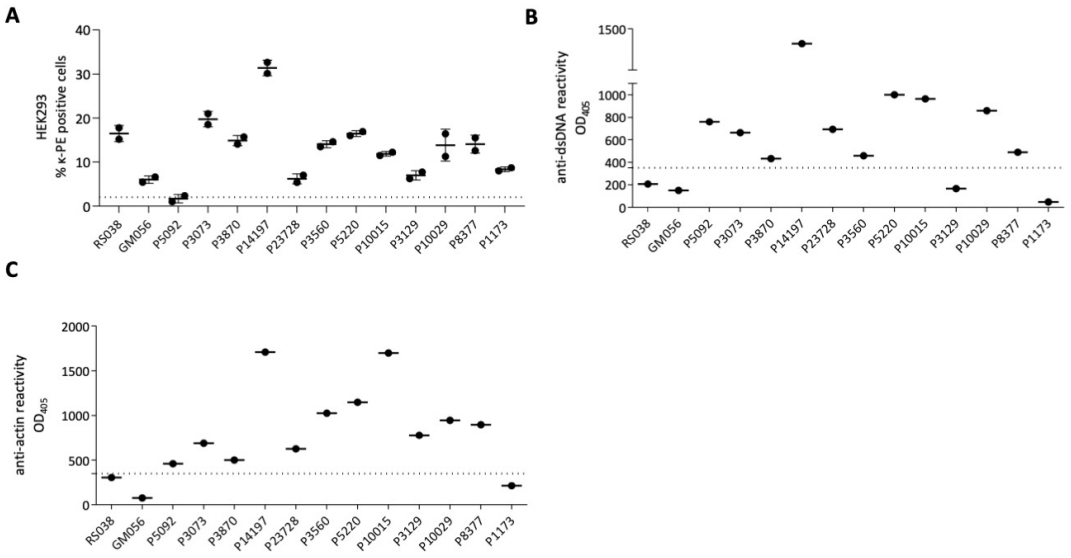

Figure S4. **Reactivity of subset 1 IgM rmAbs**. **A**, Flow cytometric analysis of the binding of subset 1 recombinant IgM monoclonal antibodies to HEK293 cells. Binding was detected by PE anti-human kappa light chain. The graph shows mean +SD binding. Each bar plot represents the mean binding of one mAb as calculated by 2-6 independent experiments. B-C, Representative polyreactivity ELISA tests of subset 1 recombinant IgM monoclonal antibodies. Reactivity against dsDNA (**B**) and actin (**C**) was tested by ELISA. In all ELISAs CLL rmAbs were used, in duplicates, as primary antibodies. Each bar corresponds to the mean OD value. The cut-off value of the weak positivity is indicated by dotted horizontal lines.

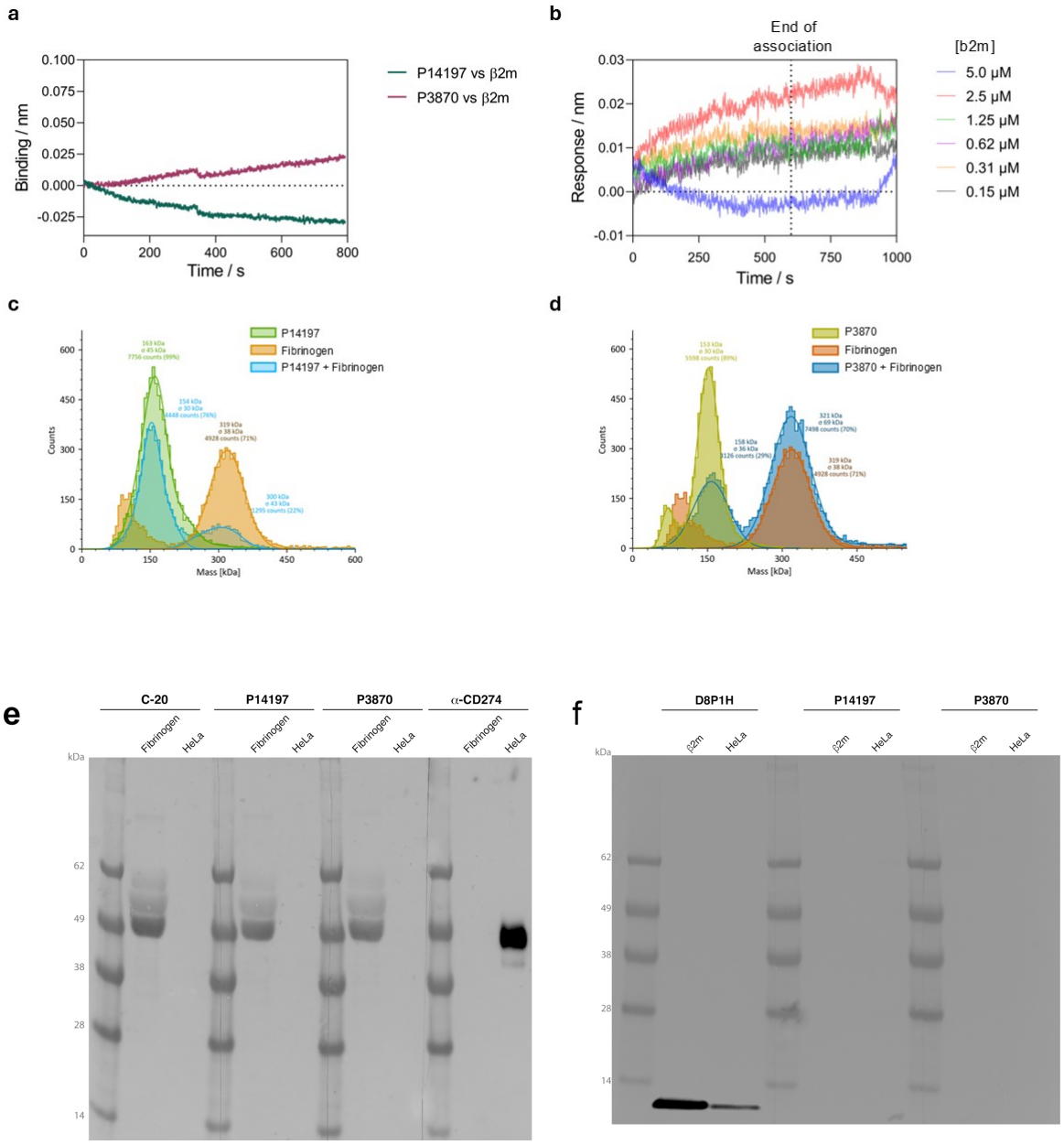

Figure S5. Reactivity of subset 1 rmAbs towards antigens identified in the microarrays. a) BLI sensograms of immobilized P14197 (green) and P3870 (red) dipped into β2-microglobulin. No interaction was observed. **b)** P14197 – β2m interaction kinetics. No binding was detected. **c)** Mass photometry analysis of P14197 (green), fibrinogen (orange), and mixture P14197-fibrinogen (cyan). No complex formation was detected. **d)** Mass photometry analysis of P3870 (yellow), fibrinogen (orange), and mixture P3870-fibrinogen (blue). No complex formation was detected. **e)** Western blot analysis shows that both subset 1 rmAbs P14197 and P3870 bind to the unfolded bovine fibrinogen IV, but not to HeLa cell extracts. The C-20 anti-fibrinogen antibody was used as a positive control. The anti-CD274 antibody recognizes a band near 49 kDa in HeLa cells extracts only. **f)** No significant reactivity of the subset 1 BCR Fabs towards β2-microglobulin is observed. For comparison, the anti-β2-microglobulin antibody D8P1H binds to both the recombinant β2-microglobulin and the protein from HeLa cell extracts.

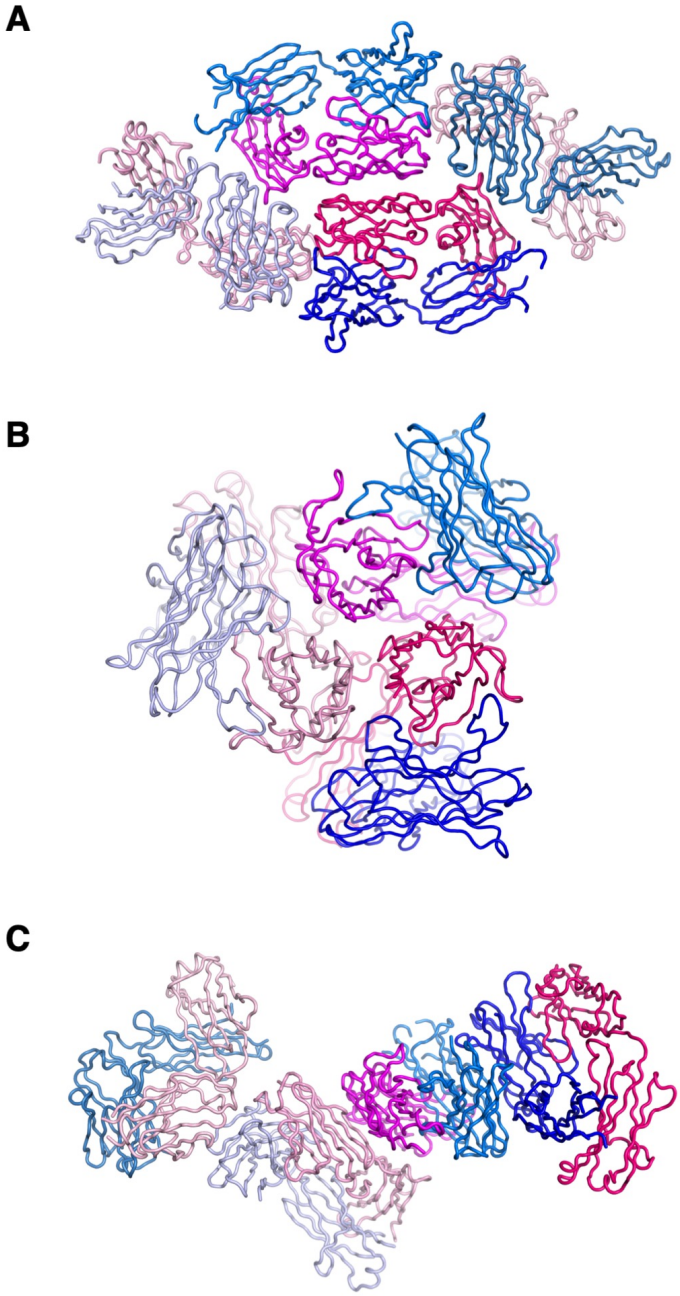

Figure S6. **Heterogeneity in the intermolecular contacts in subset 1 BCR Fab crystals.** In all panels, the heavy chains are coloured in shades of blue and the light chains in shades of pink. **A,** P3129 Fabs interact in a head-to-head fashion mediated by light chain framework residues. **B,** P10015 Fab molecules form a symmetric trimer through contracts mediated largely by the light chain. **C,** the four independent P1173 molecules form crystal contacts using either heavy or light chain residues.

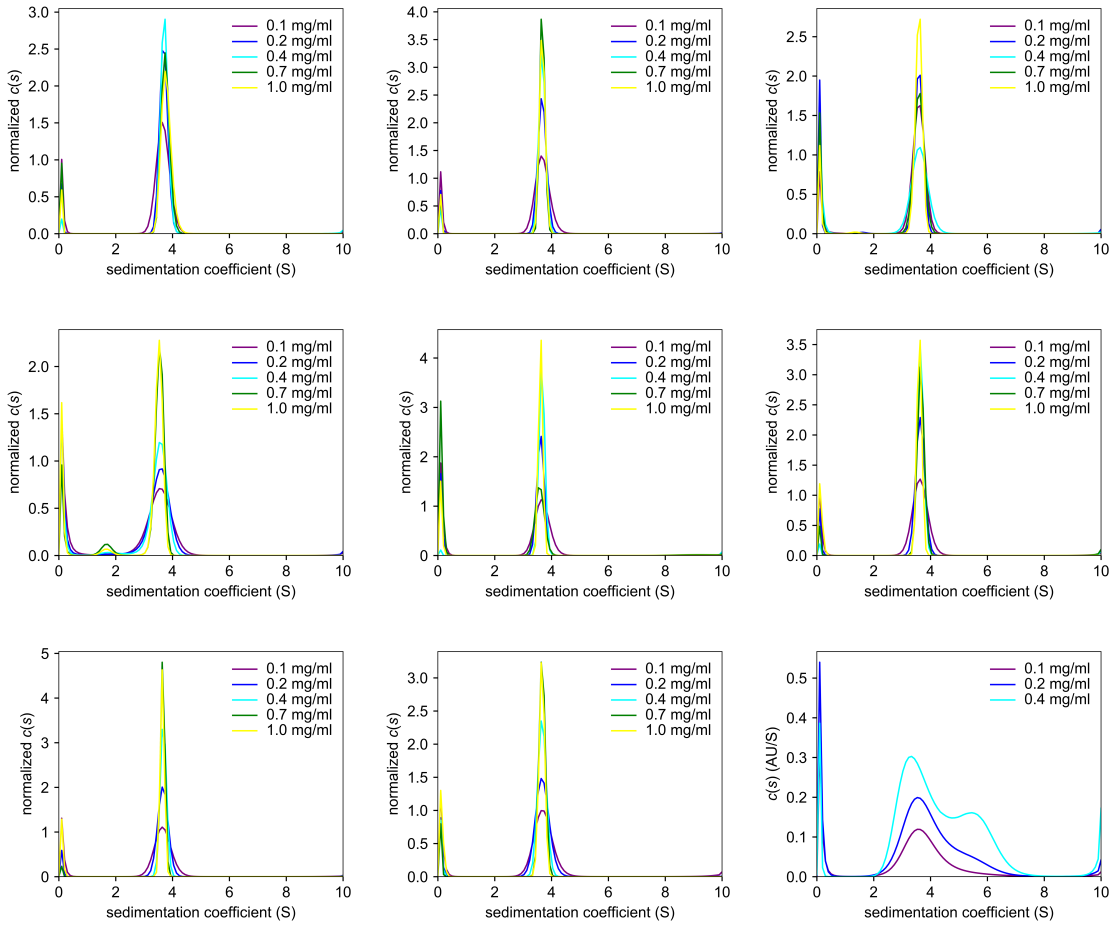

Figure S7. Analysis of self-association between CLL subset 1 BCR Fabs in solution. SV-AUC analysis of eight other subset 1 BCR Fabs (left to right, top to bottom: GM506, RS038, P3073, P3870, P5092, P5220, P23278, P14197). A dominant monomeric species at 3.8 S is apparent from the *c(s)* distributions. The SV-AUC profile for the subset 4 BCR Fab CLL240 that forms homodimers[1] is shown for comparison in the bottom right panel.

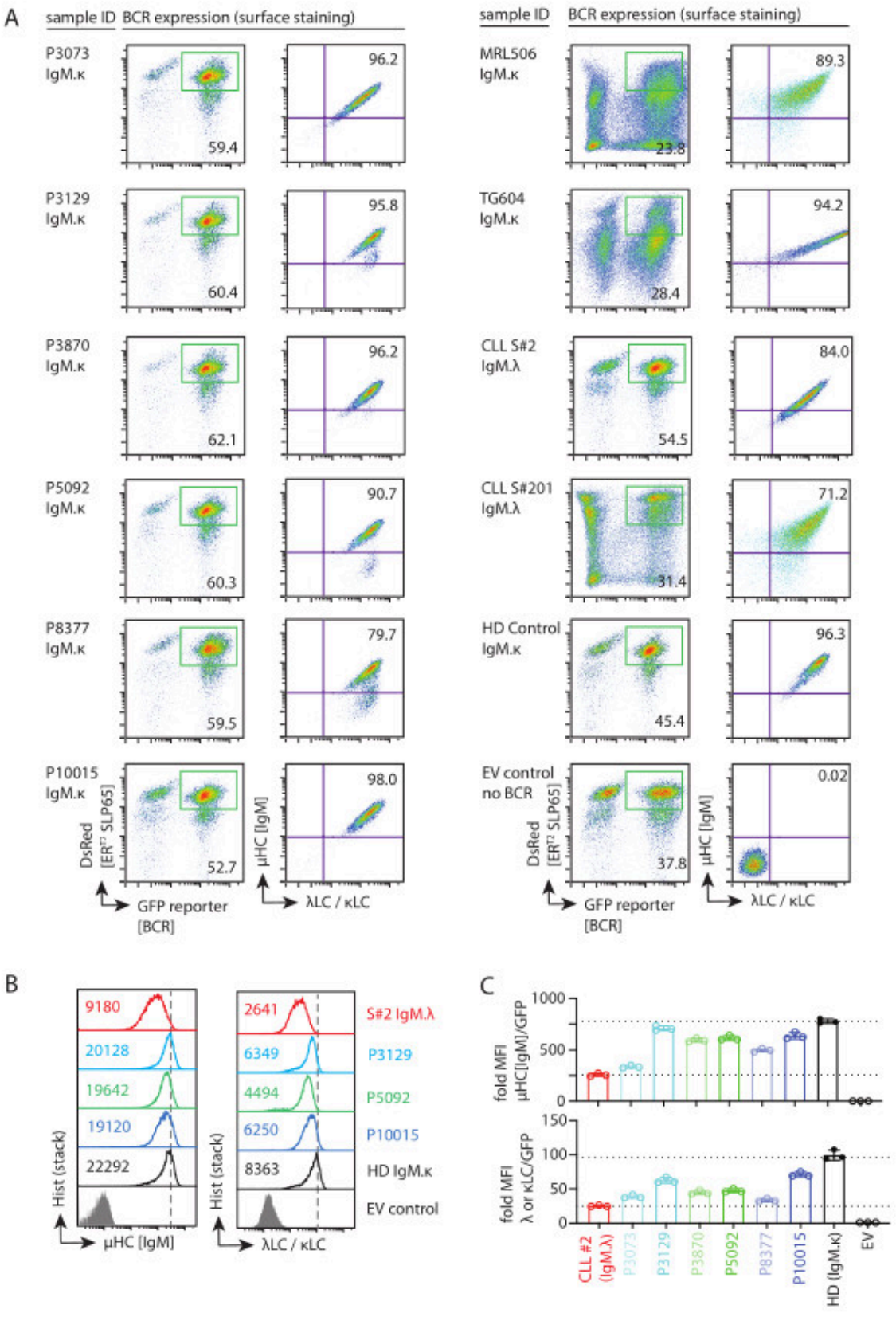
A
sample ID
BCR expression (surface staining)
P3073 IgM.κ
96.2
59.4
P3129 IgM.κ
95.8
60.4
P3870 IgM.κ
96.2
62.1
P5092 IgM.κ
90.7
60.3
P8377 IgM.κ
79.7
59.5
P10015 IgM.κ
98.0
52.7
MRL506 IgM.κ
89.3
23.8
TG604 IgM.κ
94.2
28.4
CLL S#2 IgM.λ
84.0
54.5
CLL S#201 IgM.λ
71.2
31.4
HD Control IgM.κ
96.3
45.4
EV control no BCR
0.02
37.8
DsRed [ER^T2 SLP65]
GFP reporter [BCR]
μHC [IgM]
λLC / κLC
B
9180
20128
19642
19120
22292
2641
6349
4494
6250
8363
S#2 IgM.λ
P3129
P5092
P10015
HD IgM.κ
EV control
Hist (stack)
μHC [IgM]
λLC / κLC
C
fold MFI μHC[IgM]/GFP
fold MFI λ or κLC/GFP
1000
500
0
150
100
50
0
CLL #2 (IgM.λ)
P3073
P3129
P3870
P5092
P8377
P10015
HD (IgM.κ)
EV

Figure S8. BCR expression in TKO cells. A, Representative FACS plots showing expressions of patient derived and control BCRs in TKO cells used for Ca^{2+} influx assays in Fig. 7 and S9. Left panels in each column show expressions of reporter GFP vs dsRed corresponding to BCR and inducible ERT2-SLP65 constructs, respectively. Right panels show λ or κ light chain (λ/κ LC) vs μ heavy chain (μHC) expression compared to empty vector control (right column, bottom panels). **B,** Stacked histogram showing overlay of μHC[IgM] (left panel) and λ/κ LC (right panel) expression in three subset 1 samples (sky-blue, green and indigo) compared to HD derived IgM.κ (black) and CLL subset 2 (red). Mean fluorescence intensity (MFI) values are indicated within the plots. Representative plots of three independent experiments are shown in panels A-B. **C,** Quantification of fold change in ratio of MFIs of μHC[IgM]/GFP (upper panel) and λ/κ LC/GFP (lower panel) from three independent experiments normalized to EV level. Dashed lines represent highest and lowest mean expression levels of subset 2 and healthy donor-derived BCRs, respectively.

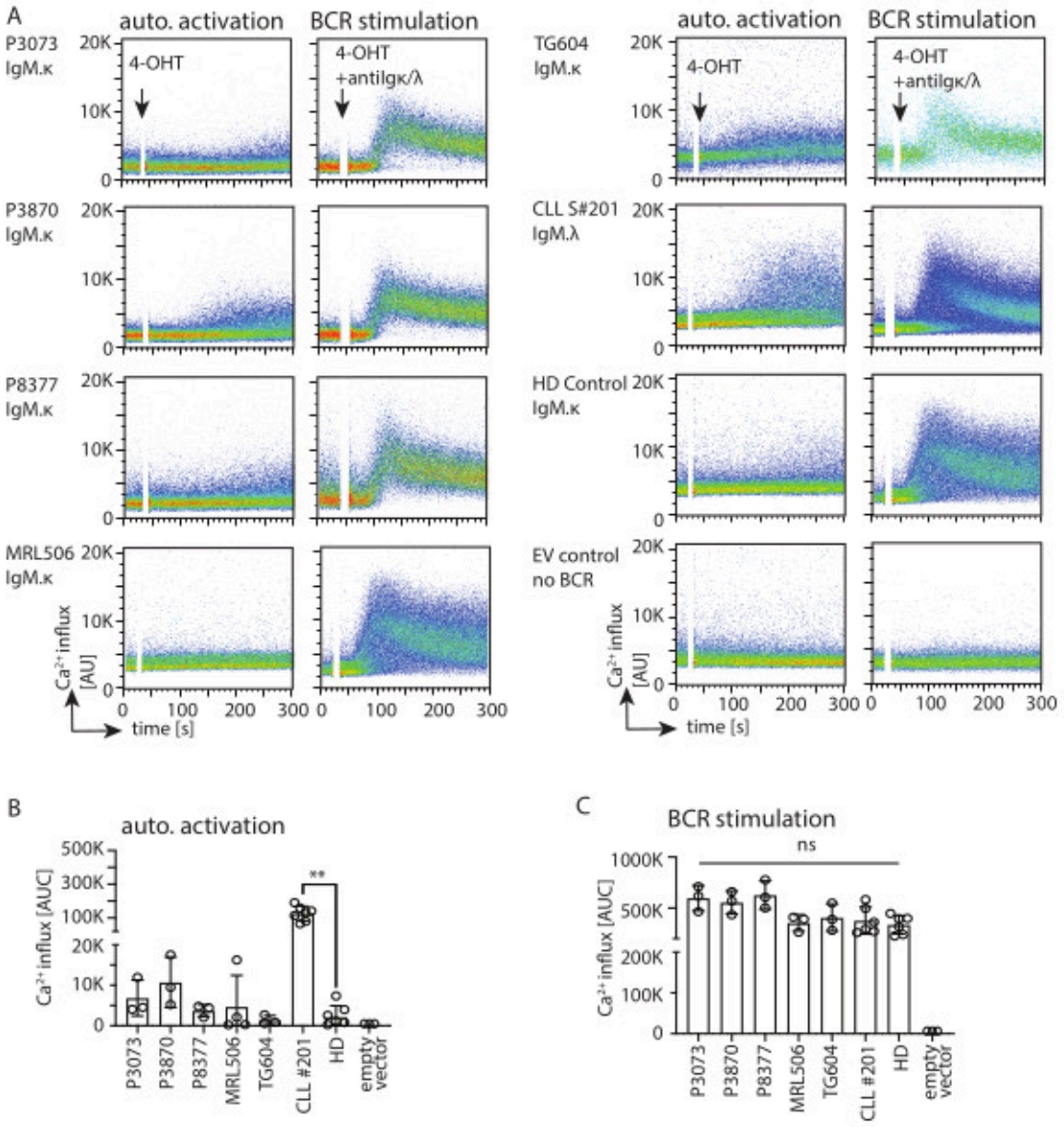

Figure S9. Defective cell-autonomous signalling of subset 1 compared to subset 201 BCRs. A, Ca^{2+} release kinetics of P3073, P3870, P8377, MRL506 (left panels) and TG604 compared to controls derived from CLL subset 201, healthy donor (HD) and no BCR (right panels) upon addition of 4-OHT ± anti-Igκ/λ antibody, revealing autonomous BCR signaling and BCR signaling capacity, respectively. BCR isotypes and associated light chain annotations are depicted for each sample. Addition of 4-OHT ± anti-Igκ/λ antibody within live sample acquisition are indicated within the plot. **B**, Bar graph shows the area under the curve (AUC) of 4-OHT induced Ca^{2+} kinetics, representing autonomous BCR signaling. **C**, Same as B, showing AUC of 4-OHT+anti-Igκ/λ antibody induced Ca kinetics representing BCR signaling strength. In panels A, B and C, results shown are representative or mean±SD of three independent experiments, showing each measurement, and analyzed by One-Way ANOVA with Welch's approximation followed by Dunnett's T3 multiple comparison. p**<0.01

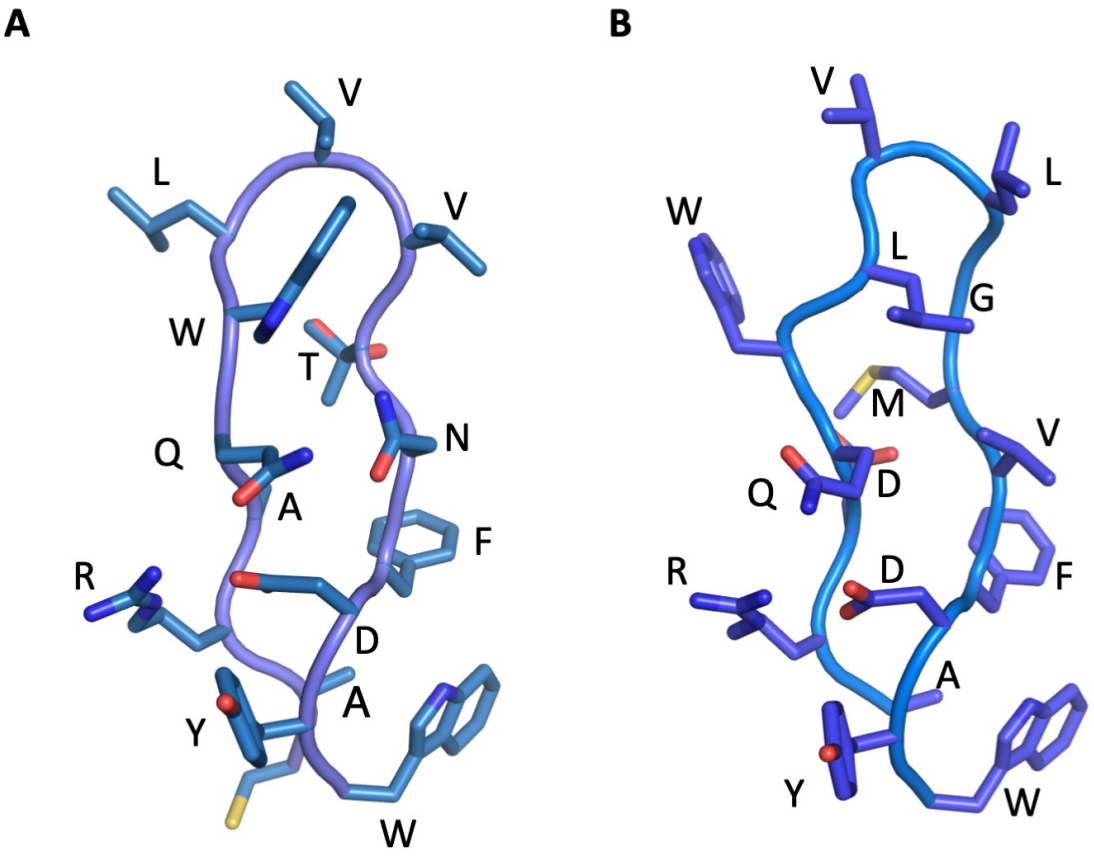

Case	Subset	HCDR3 sequence	Heavy chain gene usage
UM-CLL4	99	ARDQWLVLGMVFDYW	IGHV1-3 IGHD6-19 IGHJ4
P3129	1	AREQWLDLAH-FDYW	IGHV1-3 IGHD6-19 IGHJ4
P10015	1	ARAQWLVVTN-FDYW	IGHV1-2 IGHD6-19 IGHJ4
P1173	1	AREQWLGIKN-FDYW	IGHV5-10-1 IGHD6-19 IGHJ4

Figure S10. **Predicted structural differences between heavy chain CDR3s in subsets 1 and 99 CLL BCRs. A**, Experimental structure of the P10015 HCDR3 loop, showing the backbone as a ribbon and the side chains as sticks. **B**, Predicted structure obtained using the deep-learning algorithm implemented in ABodyBuilder2 (https://opig.stats.ox.ac.uk/webapps/sabdab-sabpred/sabpred/abodybuilder2/) of the HCDR loop of the subset 99 UM-CLL4 BCR. **C**. HCDR3 sequences of subset 1 and 99 CLL BCRs. The amino acid differences and insertion further enhance the hydrophobicity of the HCDR3 region, and are also predicted to influence the loop conformation.

Table S1. **Crystallographic data collection and refinement statistics**

	P3129	**P10015**	**P1173**
PDB ID code	9GFG	9GFF	9GFH
Data collection			
Beamline	ESRF ID30-A1	ESRF ID30-A1	ESRF ID23-1
Wavelength (Å)	0.966	0.966	0.972
Unit cell parameters (Å, °)	a=104.64, b=87.89, c=115.48, β=94.589	a=b=99.95, c=123.05, γ=120°	a=122.83, b=125.62, c=130.87
Space group	$P2_1$	$P6_3$	$P2_12_12_1$
Resolution range (Å)	115.2-2.11 (2.16-2.11)	86.57-2.51 (2.64-2.51)	90.63-1.87 (2.02-1.87)
N. of measured reflections	767,680 (51,623)	289,907 (27,206)	1,656,224 (87,597)
N. of unique reflections	120,564 (8,714)	23,294 (2,319)	123,151 (6,158)
Completeness (%)	99.8 (98.1)	99.8 (99.9)	96.2 (81.5)
Redundancy	6.4 (5.9)	12.4 (11.7)	13.4 (14.2)
$\langle I/\sigma(I)\rangle$	10.0 (0.6)	14.0 (1.2)	12.4 (1.7)
R_{merge}	0.083 (3.340)	0.103 (1.601)	0.116 (1.388)
R_{meas}	0.091 (3.660)	0.119 (1.994)	0.126 (1.494)
$R_{p.i.m.}$	0.032 (0.830)	0.043 (0.746)	0.034 (0.399)
$CC_{1/2}$	0.999 (0.238)	0.999 (0.465)	0.998 (0.666)
Refinement			
Resolution range (Å)	115.2-2.30	86.57-2.79	90.63-1.87
N. of reflections, I>0 (free set)	92,938 (4,551)	17,242 (796)	123,151 (6,054)
R_{crys}	0.220	0.204	0.174
R_{free}	0.246	0.235	0.212
rmsd bonds (Å)	0.003	0.004	0.009
rmsd angles (°)	0.630	0.690	0.900
Ramachandran statistics (% allowed, disallowed)	96.8, 0.06	94.3, 0.0	98.7, 0.06
Clashscore	1.46	1.50	2.71
Molprobity score	1.19	1.37	1.06
Average temperature factors ($Å^2$)			
Protein	81.7	86.1	68.4
Solvent	65.5	67.2	50.9

Table S2. Fv domains similarity in subset 1 BCRs.

	P3129	**P10015**	**P1173**
P3129	-	0.519 (203)	0.523 (181)
P10015	0.803 (220)	-	0.585 (192)
P1173	0.929 (119)	0.990 (220)	-

The Fv domains were pairwise superimposed Pymol (Cα atoms from heavy chain residues 1 through 119 and light chain residues 1 through 108). Above the diagonal, the rmsd values (Å) for the atoms superimposed are reported, between brackets the number of Cα atoms used in the rmsd calculation. Below the diagonal, the rmsd values calculated for the structurally homologous Cα atoms (number between brackets) in the Fv domains after superposition.

Table S3. **Conserved pairing between the heavy and light chains in subset 1 BCRs.**

	HL (°)	HC1 (°)	HC2 (°)	LC1 (°)	LC2 (°)	dc (Å)
P3129	-57.37	72.01	113.91	121.81	86.71	16.32
P10015	-59.94	72.38	114.21	122.91	83.00	16.09
P1173	-58.13	69.87	113.48	122.25	84.38	16.88

Geometric values describing the VH-VL pairing for the subset 1 BCR Fabs crystallized. No notable differences in the interaction and orientation of the variable domains is apparent. In this analysis, the H and L chains in the deposited coordinates were used. The angles and distances describing the VH-VL pairing are the ones derived from the program ABangle[2].

Table S4. Clinical data of subset 1 CLL patients' whose BCRs were analysed in the present study.

Patient Lab id	Gender	Year of birth	Date of diagnosis	Rai stage at diagnosis	Binet stage at diagnosis	Karyotype
P1173	F	1940	05/12/2002	I	A	46,XX[20]
P3129	M	1952	15/12/2003	IV	C	Not available
P10029	F	1947	09/09/2004	I	A	46,X,-X,+12[13]/46,XX[7]
P3073	F	1967	06/05/2005	IV	C	46,XX,del(6)(q21q27)[5]/46,XX[20]
P3870	M	1938	13/02/2006	0	A	46,XY[20]
P5092	M	1930	16/03/2007	III	C	46,XX,del(11)(q14)[11]/46,XY[17]
P5220	F	1934	16/04/2007	0	A	Not available
P14197	M	1960	12/03/2009	II	B	46,XY,del(13)(q12q14)[2]/46,XY[18]
P23728	M	1953	01/06/2012	IV	C	Not available
P3560	F	1950	16/01/2006	I	A	46,XX[20]
P10015	M	1950	01/11/2004	II	A	46,XY[20]
P8377	F	1974	03/02/2009	N/A	N/A	46,XX,t(9;13)(q34;q14)[5]/46,sl,add(18)(p11.3)[8]/46,sl,add(20)(p13)[3]/46,XX[2]
RS038	M	1940	01/01/1996	0	A	46,XY[8]/45,X-Y[3]
GM056	F	1943	01/07/2000	N/A	B	Not available

Table S4 (continued).

Patient Lab id	FISH del(13q) date	FISH del(13q) result	FISH del(11q) date	FISH del(11q) result	FISH trisomy 12 date	FISH trisomy 12 result	FISH del(17p) date	FISH del(17p) result
P1173	29/10/2003	NEGATIVE	29/10/2003	NEGATIVE	29/10/2003	POSITIVE	29/10/2003	NEGATIVE
P3129								
P10029	26/04/2010	POSITIVE	26/04/2010	NEGATIVE	26/04/2010	POSITIVE	26/04/2010	NEGATIVE
P3073	22/05/2008	NEGATIVE	22/05/2008	NEGATIVE	22/05/2008	NEGATIVE	22/05/2008	NEGATIVE
P3870	03/04/2006	NEGATIVE	03/04/2006	NEGATIVE	03/04/2006	NEGATIVE	03/04/2006	NEGATIVE
P5092	20/03/2007	POSITIVE	20/03/2007	POSITIVE	20/03/2007	NEGATIVE	20/03/2007	NEGATIVE
P5220								
P14197	05/02/2013	POSITIVE	05/02/2013	NEGATIVE	05/02/2013	NEGATIVE	05/02/2013	NEGATIVE
P23728								
P3560	17/01/2006	NEGATIVE	17/01/2006	NEGATIVE	17/01/2006	NEGATIVE	17/01/2006	NEGATIVE
P10015	09/11/2004	NEGATIVE	09/11/2004	NEGATIVE	09/11/2004	N/A	09/11/2004	NEGATIVE
P8377	03/02/2009	POSITIVE	03/02/2009	NEGATIVE	03/02/2009	NEGATIVE	03/02/2009	NEGATIVE
RS038	05/06/2008	POSITIVE	05/06/2008	POSITIVE	05/06/2008	NEGATIVE	05/06/2008	POSITIVE
GM056	02/02/2009	POSITIVE	02/02/2009	POSITIVE	02/02/2009	NEGATIVE	02/02/2009	POSITIVE

Table S4 (continued).

Patient Lab id	TP53 status examined	TP53 mutation status	Other malignant neoplasms	Other non-hematological malignant neoplasms	Other non-hematological neoplasm diagnosis	Transformation	Type of transformation	Transformation date
P1173	NO		NO			NO		
P3129	YES	Unmutated	NO			NO		
P10029	YES	Unmutated	NO			NO		
P3073	NO		YES	YES	Cervix uteri	YES	Richter Syndrome	17/03/2009
P3870	YES	Mutated	YES	YES	Prostate	NO		
P5092	NO		YES	YES	Other malignant neoplasms of skin	NO		
P5220	YES	Unmutated	N/A					
P14197	YES	Unmutated	NO			NO		
P23728	YES	Unmutated	NO			NO		
P3560	YES	Unmutated	N/A					
P10015	YES	Unmutated	N/A			YES	Richter Syndrome	14/03/2010
P8377	YES	Unmutated	N/A			NO		
RS038	NO		N/A			NO		
GM056	NO		N/A			NO		

Table S4 (continued).

Patient Lab id	Treatment status	Date of first treatment	Response to first treatment	Type of first treatment	Date of last follow-up	Survival status	Treatment status	Date of first treatment	Response to first treatment
P1173	Treated	15/01/2004	PR	Chlorambucil-single	19/07/2016	Dead	Treated	15/01/2004	PR
P3129	Treated	07/01/2004	Progressive		12/11/2005	Dead	Treated	07/01/2004	Progressive
P10029	Treated	11/07/2011	PR	Chlorambucil+Rituximab	02/10/2020	Alive	Treated	11/07/2011	PR
P3073	Treated	18/07/2005	CR	Fludarabine+Cyclophosphamide+Rituximab	15/04/2009	Dead	Treated	18/07/2005	CR
P3870	Untreated				18/05/2019	Alive	Untreated		
P5092	Treated	17/05/2007	Stable	Fludarabine+Rituximab	09/01/2012	Dead	Treated	17/05/2007	Stable
P5220					06/06/2007	Alive			
P14197	Treated	17/04/2013	PR	Fludarabine+Cyclophosphamide+Rituximab	27/02/2024	Alive	Treated	17/04/2013	PR
P23728	Treated	01/06/2012	PR	Bendamustine+Obinutuzumab	17/01/2024	Alive	Treated	01/06/2012	PR
P3560	Treated	10/04/2006	PR	Fludarabine+Cyclophosphamide+Rituximab	18/06/2024	ALIVE	Treated	10/04/2006	PR
P10015	Treated	02/12/2009	PR	Fludarabine+Cyclophosphamide+Rituximab	07/09/2010	Dead	Treated	02/12/2009	PR
P8377	Untreated				23/05/2011	Alive	Untreated		
RS038	Treated	01/09/2005	PR	Chlorambucil-single	10/02/2011	Dead	Treated	01/09/2005	PR
GM056	Treated	01/02/2001	N/A	Chlorambucil-single	27/12/2010	Dead	Treated	01/02/2001	N/A

Additional references.

1. Minici, C. *et al.* Distinct homotypic B-cell receptor interactions shape the outcome of chronic lymphocytic leukaemia. *Nat Commun* **8**, 15746 (2017).
2. Dunbar, J., Fuchs, A., Shi, J. & Deane, C. M. ABangle: characterising the VH–VL orientation in antibodies. *Protein Engineering, Design and Selection* **26**, 611–620 (2013).